Proceedings of the 12th International Conference on
Environmental Degradation of Materials in Nuclear Power System – Water Reactors –
Edited by T.R. Allen, P.J. King, and L. Nelson ***TMS (The Minerals, Metals & Materials Society), 2005***

Corrosion of Zirconium-based Fuel Cladding Alloys in Supercritical Water.

Y.H. Jeong[1], J.Y. Park[1], H.G. Kim[1], J. T. Busby[2], E. Gartner[2], M. Atzmon[2], G. S. Was[2], R.J. Comstock[3], Y.S. Chu[4], M. Gomes da Silva[5], A. Yilmazbayhan[5] and A.T. Motta[5]

[1]Zr Fuel Cladding Team, Korea Atomic Energy Research Institute, Daejeon 305-353, Republic of Korea
[2]Dept. of Nuclear Engineering and Radiological Sciences, University of Michigan, Ann Arbor, MI 48109-2104, USA
[3]Science and Technology Dept., Westinghouse Electric Co., Pittsburgh, PA 15235-5082, USA
[4]Advanced Photon Source, Argonne National Laboratory, Argonne, IL, 60439, USA
[5]Dept. of Mechanical and Nuclear Engineering, The Pennsylvania State University, University Park, PA 16802, USA.

Keywords: Zirconium alloys, corrosion, supercritical water

Abstract

Corrosion tests in supercritical water and 500°C steam were performed on Zr-based model alloys up to 132 days to evaluate the potential use of Zr alloy cladding in the supercritical water reactor (SCWR). Corrosion tests performed in dynamic and static conditions showed similar results, and the 500°C steam test also showed promise as a screen test for supercritical water as the relative corrosion behavior of the alloys appeared to be similar. The corrosion test results showed a wide variety of corrosion resistance depending on the alloy composition. While Zr sponge, crystal bar Zr and Zircaloy-4 showed accelerated corrosion behavior, some of the experimental model alloys showed appreciable corrosion resistance. Among the alloys that exhibited reasonable corrosion resistance the best were Zr-Fe-Cr or Zr-Cr-Fe alloys, and these compared favorably with other alloys under consideration for the SCWR, such as ferritic-martensitic alloys. The results suggest that at least as far as uniform corrosion goes, Zr alloys could be considered for utilization in the supercritical water cooled reactor

Introduction

The supercritical water cooled reactor (SCWR) is being proposed as part of the Generation IV reactor concept. The SCWR will have fuel designs similar to current light water reactor (LWR) but operate at considerably higher temperatures. The materials to be used for the fuel cladding and reactor internals in the SCWR have not been defined. The use of Zr-based alloys would bring a clear neutronics benefit, at least for the thermal SCWR version. Waterside corrosion is a limiting factor in the operation of Zr-based fuel cladding in current LWRs and would be a much greater concern in the SCWR.

A significant hurdle for the utilization of zirconium alloys in SCWR is the higher corrosion rate that would be expected at the higher operating temperatures envisaged for these reactors. In the reactor, under heat flux conditions, the situation is worse, as the growing oxide layer serves as a barrier to heat flow, further increasing the temperature at the oxide-metal interface. Since the heat transfer to the superheated coolant is less efficient than that for water, the peak cladding temperature is significantly higher than the average outlet coolant temperature. Finally, the hydrogen pickup fraction could be as high as 44% at 500-550°C [1], which is much higher than the typical hydrogen pickup fraction of 15% at LWR temperatures.

Although these obstacles are formidable, the advantages of having a cladding material that is more neutron transparent than the current alloys proposed for the SCWR (Inconels and steels) are significant. The fuel enrichment could be significantly decreased from the currently envisaged 7.5%, with a corresponding decrease in operational costs and possible simplification of licensing procedures. The removal of parasitic poisons from the cladding would allow greater core design flexibility. The possible use of Zr alloys in SCWR is not restricted to the fuel cladding. The low moderator density in the high temperature region may require the use of moderators such as water rods, or Zr hydride plates. Such moderating rods would have to be clad, and if an absorbing material were used, a significant penalty would have to be paid. The use of Zr alloys for such rods would be easier to achieve because in the absence of heat flux, the peak cladding temperatures would be approximately equal to the average coolant outlet temperature.

The database on the corrosion of zirconium-based alloys in supercritical water is virtually nonexistent, although it was reported that Zr-Cr and Zr-Cu based alloys with a high volume fraction of second phase particles showed promise in improving high temperature corrosion resistance relative to Zircaloy-2 and Zircaloy-4 [2-4]. In this investigation, corrosion tests in supercritical water and 500°C steam were performed on Zr-based model alloys to evaluate the potential use of Zr alloy cladding in the SCWR.

Experimental Methods

The alloys used in this study are shown in Table 1. The experimental alloys can be classified into four groups according to the alloy system; Zr-Nb, Zr-Fe-Cr, Zr-Cr-Fe and Zr-Cu-Mo alloys. Two types of pure Zr, i.e., sponge Zr and crystal bar Zr, as well as Zircaloy-4 were used as reference alloys. All of the experimental alloys were designed to investigate the effect of precipitates on corrosion, with the exception of Zr-Nb alloys containing less than solubility limit of Nb (Zr-0.2Nb and Zr-0.4Nb) which was intended for examining the solute element effect.

The experimental alloys were prepared by arc-melting, remelting at least four times to promote chemical homogeneity. A typical arc-melted button measures about 70 mm in diameter and 10 mm in thickness, and weighs about 400 g. The arc-

melted ingots were beta-solution treated at 1050°C for 30 min in a vacuum furnace, hot-rolled after pre-heating at 580 to 720°C for 10 min and cold-rolled three times to a final thickness of 0.8 mm. Between the rolling steps, the cold-rolled sheets were intermediate-annealed at 580 to 720°C depending on the alloy system.

The microstructures of the manufactured alloys were characterized by optical microscopy to ensure that the alloys had homogeneous microstructures. For a given series, the grain size of the alloys decreased with increase of alloying element. The model alloy samples were systematically examined using synchrotron radiation x-ray diffraction at the 2-BM beamline of the Advanced Photon Source (APS) to determine the structure and volume fraction of precipitates present following the method in [5].

The microstructures of the alloys were also examined using a transmission electron microscope (TEM) equipped with an energy dispersive X-ray spectrometer (EDS). Specimens for TEM observation were prepared by a twin-jet polishing with a solution of 10 vol.% $HClO_3$ and 90 vol.% C_2H_5OH after mechanical thinning to 70 μm. Selected area diffraction patterns (SADP) were obtained and analyzed to determine the crystal structure of the precipitates, and micro-chemical analyses on the precipitates were conducted using EDS.

Specimens for corrosion testing, 25 by 20 by 0.8 mm in size, were cut from the manufactured strip, mechanically ground up to 1200 grit SiC paper, and then pickled in a solution of 5 vol.% HF, 45 vol.% HNO_3 and 50 vol.% H_2O. The corrosion tests were conducted in 500°C/1500psi steam and 500°C/3650psi supercritical water (SCW) in a manner consistent with the ASTM Practice (G2-88). The corrosion behavior of the specimens was evaluated by measuring the weight gain as a function of the exposure time. The corrosion test in supercritical water was performed in two types of facilities; one is a static autoclave (closed environment in which water does not recirculate) at KAERI and the other is a dynamic loop system (water is constantly refreshed, and chemistry is controlled) at University of Michigan. The 500°C steam corrosion test was performed at Westinghouse in a static autoclave at 1500 psi. In all cases the water environment was deaerated, maintaining the oxygen content lower than 40 ppb.

In the dynamical supercritical loop system, the water system was cleaned and purified prior to heating up the autoclave. Both inlet and outlet conductivity were below 0.1 μS/cm prior to heating. Similarly, the oxygen content was measured at < 10 ppb at both the inlet and outlet. The flow rate was 12 ml/min. After heating to supercritical conditions, the outlet conductivity rose rapidly to 0.6 μS/cm where it stayed throughout the test, while the inlet conductivity remained at 0.1 μS/cm, indicative of high corrosion rates. All experimental parameters were monitored continuously by a computer with the LabVIEW software.

Results and discussion

Metallurgical characterization

The as-fabricated model alloys were characterized using synchrotron radiation x-ray diffraction to identify second phases present. One example of such an examination is shown in Figure 1, where the x-ray intensity is plotted versus two theta angle acquired using an x-ray energy of 17 keV, for the examination of the alloys Zr-0.4Fe-0.2Cr and Zr-0.2Fe-0.1Cr, processed at 580°C (indicated as L for low temperature heat treatment) and 720°C (indicated H for high temperature heat treatment). The vertical scale is logarithmic to highlight in greater detail the small second phase peaks, which comprise only a small fraction of the total sample volume. The advantage of performing these experiments at the APS synchrotron facility is that the high photon flux (orders of magnitude higher than conventional sources) and low background permits detection of small diffraction peaks. Thus, second phase volume fractions as low as 0.1 to 0.2% can be detected. In Figure 1, these capabilities are well illustrated. In the upper part of the figure, the pattern obtained from the samples processed at 580 C is shown. The heavier weight line corresponds to the Zr-0.2Fe-0.1Cr alloy and the lighter weight line to the Zr-0.4Fe-0.2Cr alloy. At both annealing temperatures is noticeable that the intensity from the second phase particles is higher in the alloy with higher alloying element content. The second phase peaks correspond to the $Zr(Cr,Fe)_2$ C15 cubic $MgZn_2$ Laves phase type structure, while for the higher processing temperature the second phase peaks correspond to the $Zr(Cr,Fe)_2$ C14 $MgCu_2$ Laves phase type structure. It is also noticeable that the peaks for the cubic precipitate phase are broader than those for the hexagonal phase. The peak heights are similar for the equivalent alloying content at both processing temperatures suggesting that the alloying elements have precipitated out. This is as expected, since their solubilities in the alpha-Zr matrix are very low. Although the stable precipitate structure for the Fe/Cr ratio present in the alloy is the C14 hcp structure the precipitates form at first with a cubic structure, likely due to the stabilization of the C15 phase by the small precipitate size or by compositional variations (it is known that for either very high or very low Fe/Cr ratio the C15 phase is more stable [6]). Thus, as the alloys are annealed the precipitates grow and change crystal structure. In this particular case, it is possible to study and characterize the precipitate structure, volume fraction and size independently. By preparing such controlled microstructures we can investigate the influence of each parameter independently.

Similar characterization was performed for all the alloys studied. The results are summarized in Table 1. The precipitates diameters shown in Table 1 were calculated using the Scherrer formula as was done in [5]. All alloys considered for this study formed second-phase precipitates with the sole exception of Zr-0.2Nb and Zr-0.4Nb alloys, which have a Nb concentration below the solubility limit in α-Zr. The types of second phase precipitates were: (i) of the C14 hcp $Zr(Cr,Fe)_2$ type in the ZrFeCr and ZrCrFe alloys (with the exception of the low temperature processed materials which exhibited cubic C15 type Laves phase precipitates of similar composition) , (ii) bcc β-Nb and hcp $(Zr,Nb)Fe_2$ precipitates in the Zr-Nb alloys

(Fe is an impurity in these alloys at 100-600 ppm) (iii) cubic C15 $ZrCu_2$ and hcp C14 $ZrMo_2$ type in the ZrCuMo alloys and (iv) the usual precipitates in Zircaloy-4 [7]. No precipitates were detected in either sponge or crystal bar Zr, and the detection limit is estimated at <0.1%. The different processing temperatures in the ZrFeCr alloys created alloys with small and large precipitates and the two compositions gave different volume fractions. We should also note that Zr-Sn and Zr-SnNb

Table 1. Characteristics of as-fabricated model alloys used in this study

Alloy system	Composition (wt.%)	Second Phase Particle Characteristics		
		Type	size (nm)	Volume Fraction
Zr-Nb	Zr-0.2Nb, Zr-0.4Nb, Zr-1.0Nb, Zr-1.5Nb, Zr-2.5Nb	Hex. $Zr(Nb,Fe)_2$, bcc β-Nb and orthor. Zr_3Fe	75-110	Increases as Nb content increases (0-2.3%)
Zr-Fe-Cr	Zr-0.4Fe-0.2Cr (580 °C (L) and 720 °C (H) processing temp.)	$Zr(Cr,Fe)_2$ Cubic (L) and hcp (H)	35 (L) 107(H)	~1%
Zr-Cr-Fe	Zr-0.5Cr-0.2Fe, Zr-1.0Cr, Zr-1.0Cr-0.2Fe	Cubic $ZrCr_2$ and cubic $Zr(Cr,Fe)_2$	40-60	~1-1.5%
Zr-Cu-Mo	Zr-0.5Cu, Zr-1.0Cu, Zr-1.0Cu-0.5Mo	Tetragonal Zr_2Cu and cubic $ZrMo_2$	> 100	~0.5-2%
Reference Alloys	Pure Zr (sponge and crystal bar), Zircaloy-4	no precipitates for Zr $Zr(Cr,Fe)_2$ for Zircaloy-4	80	~0.5 for Zircaloy-4

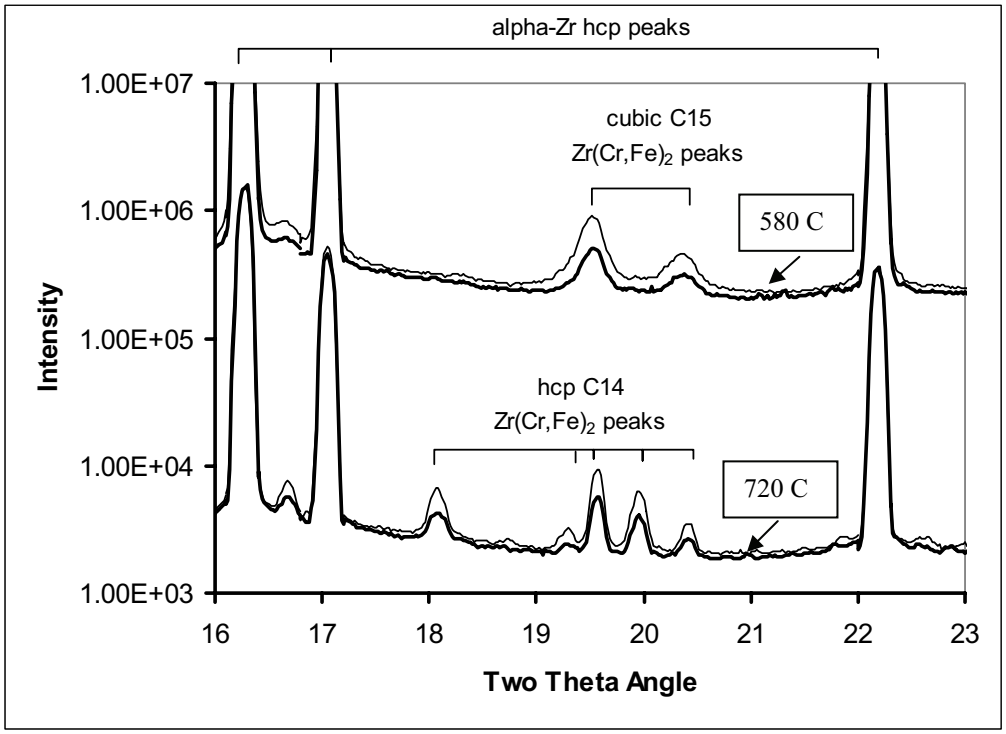

Figure 1: Diffracted intensity versus two-theta angle (logarithmic scale) for two Zr-Fe-Cr alloys (Zr-0.2Fe-0.1Cr and Zr-0.4Fe-0.2Cr) processed at at two different temperatures (580 and 720 C) obtained with synchrotron radiation for the purpose of identification of second phase particles phases present in the alloy.

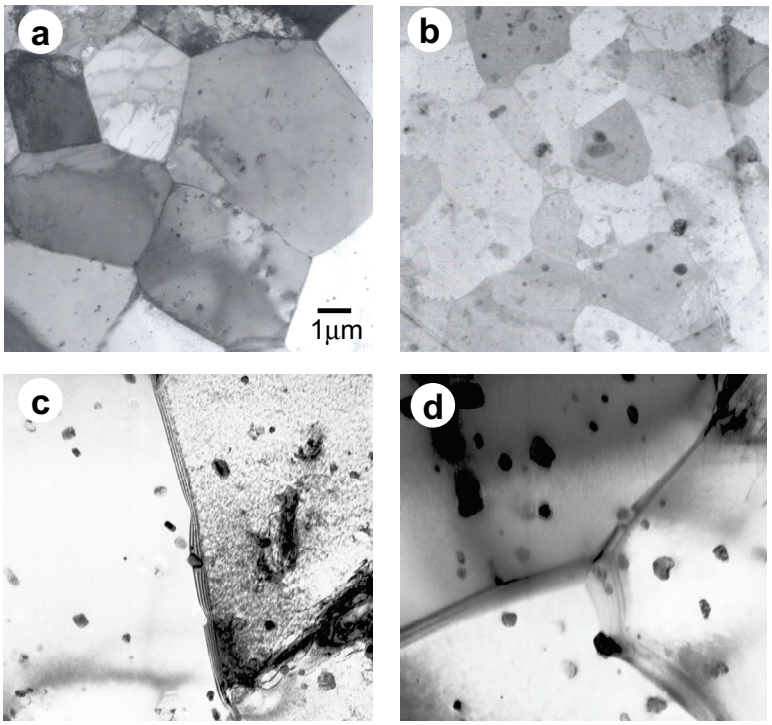

Figure 2. Bright field TEM micrographs showing the microstructures of as-fabricated model alloys: (a) Zr-0.4Nb, (b) Zr-1.5Nb, (c) Zr0.5Cr0.2Fe and (d) Zr-0.5Cr.

samples were tested but behaved poorly in this test, showing evidence of nodular corrosion and of breakaway behavior at an early stage.

Examinations of the samples using TEM confirmed the results above and showed that a homogeneous microstructure was achieved for the alloys used in this work, as shown in Figure 2.

Corrosion behavior in supercritical water

In this section the results of long term corrosion tests in static autoclaves are shown. As expected, both sponge Zr and the crystal bar Zr were very susceptible to corrosion in the supercritical water. After one day exposure, the entire corrosion specimens of pure Zr changed to white oxide and they were pulverized with only a small force applied. Zircaloy-4 also showed a weight gain of more than 2500mg/dm^2 after just 1 day. Because approximately 14.7 mg/dm^2 in weight gain corresponds to 1 micron of oxide this corresponds to 170 microns of oxide.

The corrosion weight gain measured in the alloys of the Zr-Nb system is shown in Figure 3. The weight gains are similar for all the alloys with more than 0.2 Nb, and the oxide appears to be protective for over 130 days, although with a reasonably high corrosion rate.

The corrosion behavior of Zr-Nb alloys in 500°C steam and supercritical water was approximately the same. The exception to this group was the Zr-0.2Nb alloy which showed breakaway behavior and oxide spalling in the early stages of corrosion in both corrosion environments, showing a weight gain of 1793mg/dm^2 after 1 day and an oxide that was entirely white. Overall, the corrosion rate of Zr-Nb alloys in supercritical water was twenty times higher than that in 360°C pure water [8]. Among the alloys with Nb greater or equal to 0.4, it was found that the corrosion resistance in supercritical water increased slightly with Nb content.

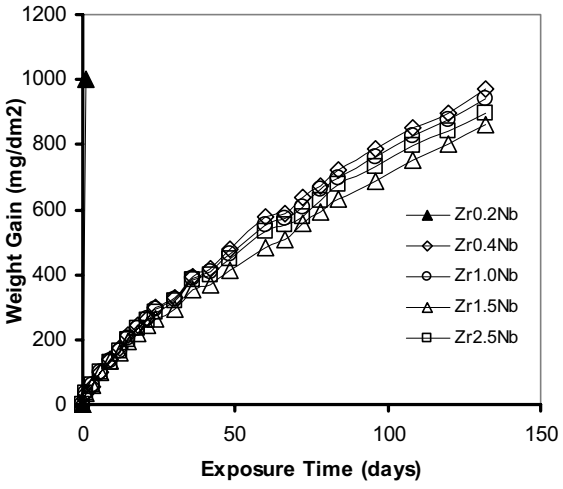

Figure 3: Weight gain versus exposure time in 500°C supercritical water for Zr-Nb alloys.

The alloy with a higher amount of second phase would be more corrosion resistant in supercritical water condition as compared to the alloy with lower amount of alloying elements. It was known that the corrosion resistance of Zr-Nb alloys is highly dependent on the characteristics of the second phase particles such as size distributions and crystal structures [9]. In this investigation, the Zr-Nb alloys with a high Nb content have beta-Nb as second phases whose density increases with Nb content. The control of the precipitation of beta-Nb is crucial to improve the corrosion resistance of Zr alloys in 360°C water [8]. The Zr-Nb alloys heat treated at 580°C to form beta Nb as precipitates showed much better corrosion resistance than the alloys heat treated at 640°C and which formed β-Zr. The presence of β-Nb was expected to be effective to improve the corrosion resistance of Zr-Nb alloys in supercritical water condition. The corrosion resistance increased with an increasing amount of the beta-Nb up to 1.5wt.% Nb and then decreased with Nb contents from 1.5 to 2.5wt.%. Zr-2.5Nb contained a certain amount of β-Zr together with beta-Nb. The slight decrease of corrosion resistance in Zr-2.5Nb may be due to the presence of beta-Zr provided that the effect of precipitate characteristics on the corrosion of Zr-Nb alloys is same in 360°C and supercritical water.

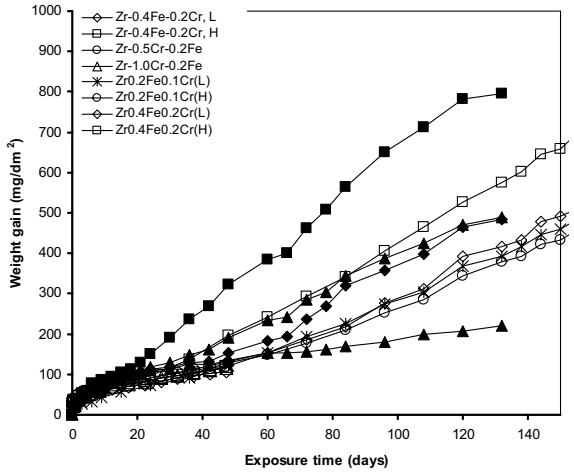

Figure 4: Weight gain versus exposure time in 500°C supercritical water and in 500°C steam for Zr-Fe-Cr alloys. Open symbols indicate corrosion in steam while closed symbols indicate corrosion in SCW.

Figure 4 shows the corrosion weight gain of Zr-0.4Fe-0.2Cr alloys in 500°C steam (open symbols) and in supercritical water (filled symbols). In contrast to the Zr-Nb alloys, these alloys showed a higher corrosion rate in supercritical water than in 500°C steam . The Zr-Fe-Cr alloys were processed at 580°C and 720°C to change the precipitate size. The alloys processed at a lower temperature showed a slightly better corrosion resistance in both conditions. It is not clear yet how reproducible these results are, and whether these differences simply result from minor variations in alloy structure, since variations of up to 30 % were seen between the test results of alloys melted in the US and in Korea. If true, the present results are not consistent with the previous result by Barberis et al. [10] who performed corrosion tests at 500°C steam for the Zr alloys with a variety of precipitate sizes and who observed that larger precipitate sizes provide better corrosion resistance in Zr-Fe-Cr alloys.

Figure 5 shows the corrosion weight gains of Zr-Cr-Fe alloys versus exposure time in supercritical water. This group of alloys showed some of the best corrosion behavior in SCW among all the alloys considered. The beneficial effect of Fe is clear, comparing the corrosion results of ZrCr and ZrCrFe. The beneficial effect of higher alloying additions is also clear. The Zr-1.0Cr-0.2Fe alloy showed the highest corrosion resistance among the Zr-Cr-Fe alloys tested. Zr-1.0Cr-0.2Fe showed a weight gain of 220 mg/dm^2 at 132 days while Zr-1.0Cr and Zr-0.5Cr-0.2Fe exhibited higher weight gains of 384 mg/dm^2 and 328 mg/dm^2, respectively. Compared to Zr-0.4Fe-0.2Cr processed at 580°C, Zr-1.0Cr-0.2Fe showed less than one half of the weight gain of Zr-0.4Fe-0.2Cr at 132 days exposure. This suggests that the higher Cr content provides a meaningful improvement to the corrosion resistance. However, Zr-Fe-Cr ternary alloys showed better corrosion resistance than the binary Zr-Cr alloys, suggesting that Fe additions also improve the corrosion resistance of Zr-Cr binary alloys.

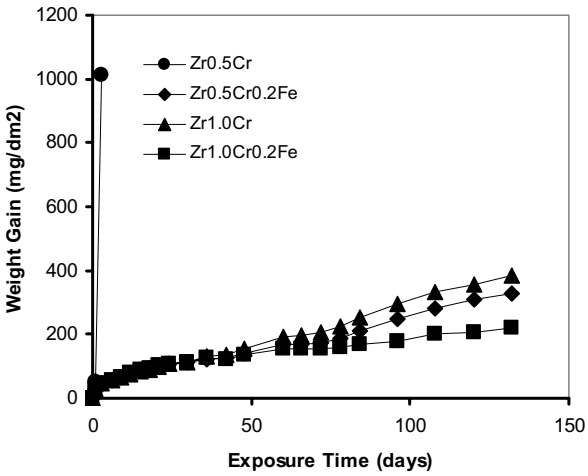

Figure 5: Weight gain versus exposure time in 500°C supercritical water for Zr-Cr-Fe alloys.

Figure 6 shows the weight gains of Zr-Cu-Mo alloys versus exposure time in supercritical water. The Zr-Cu alloys showed protective behavior throughout the test, but their weight gain was somewhat higher than for the Zr-Cr-Fe alloys. Also, compared to the Zr-Cr-Fe alloys the Cu containing alloys showed what appear to be oxide transitions around 40 days and again at around 80 days, while the Zr-Cr-Fe alloys showed no measurable changes in corrosion rate. The higher Cu content alloy (Zr-1.0Cu) showed marginally better corrosion resistance than the Zr-0.5Cr alloy, in agreement with the general trend of higher alloying element content

being beneficial to corrosion resistance at elevated temperatures.

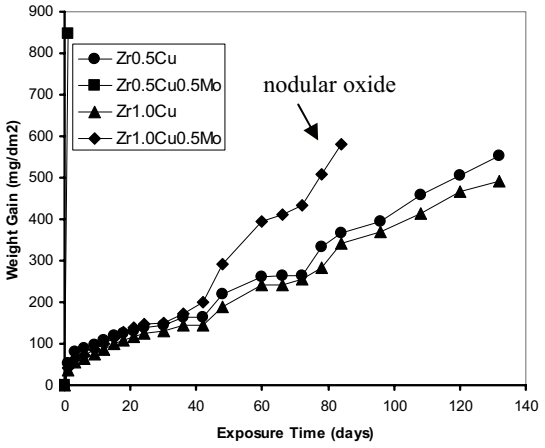

Figure 6: Weight gain versus exposure time in 500°C supercritical water for Zr-Cu-Mo alloys.

The weight gain in the Zr-1.0Cu alloys was 284 mg/dm^2 at 78 days, equivalent to about 20 microns of oxide. The presence of Mo had a deleterious impact on the corrosion resistance of the material, causing nodular corrosion and increasing the overall weight gain. The Zr-0.5Cu-0.5Mo oxide exhibited non-protective behavior from the start of the test. The Zr-1.0Cu-0.5Mo alloy showed protective behavior, but later developed nodular oxide and increased corrosion rate. In contrast, the Zr-1.0Cu alloys maintained a uniform oxide with a trace of locally accelerated corrosion up to 132 days exposure. Mo was also found to be detrimental to manufacturing the alloys when it was processed at 580°C. Mo-containing alloys were susceptible to edge cracking of the strip during the cold rolling step. This could be caused by the difficulty to homogenize the microstructure of Mo-containing alloys at the low annealing temperature of 580°C.

Comparison of the static autoclave with the dynamic loop system

Most of the corrosion data presented in this study was generated using a static autoclave system, but tests were also conducted using a dynamic loop system. The initial water chemistry was identical between the two conditions except for the fact that the dynamic loop system was operated with a refreshed environment. The question of whether there is a significant difference between supercritical water corrosion tests in a dynamic loop system and in a static autoclave needs to be addressed. The alloys in this study were tested in SCW in the dynamic autoclave for up to nine days. Zr-Fe alloys typically exhibited the best performance, with Zr-0.4Fe-0.2Cr (720° C process temperature) and Zr-0.2Fe-0.1Cr (580° C process temperature) showing weight gains of under 63 mg/dm^2 after 9 days. The best Zr-Cr based alloys in the recirculating autoclave were Zr-0.5Cr-0.2Fe and Zr-1.0Cr-0.2Fe, which exhibited weight gains of 65-73 mg/dm^2 after 9 days.

In general, the alloys that behaved poorly in the static autoclave also behaved poorly in the dynamic system; the alloys that behaved well also corresponded between the two systems but with slight differences in rate. The alloys surviving to nine days without breakaway corrosion in the dynamic autoclave were: Zr-0.2Fe-0.1Cr, and Zr-0.4Fe-0.2Cr (both process temperatures), , Zr-0.5Cr-0.2Fe, and Zr-1.0Cr-0.2Fe.

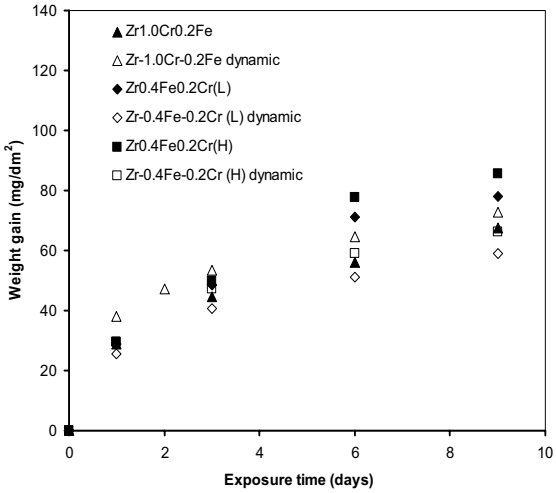

Figure 7: Comparison of weight gain versus exposure time for ZrCrFe and ZrFeCr alloys, in supercritical water at 500°C for dynamic and static autoclave systems.

Figure 7 shows the weight gain of Zr-Cr-Fe and Zr-Fe-Cr alloys to nine days. The open symbols correspond to the weight gains during SCW corrosion in the dynamic autoclave and the closed symbols to the equivalent data obtained using a static autoclave (data plotted in Figs. 4 and 5). Two of the alloys exhibit slightly lower weight gain in the dynamic autoclave compared to the static system while the other shows the opposite. In general, the results are quite comparable and indicate no bias towards either autoclave system producing higher weight gain. It is concluded that no significant differences in corrosion behavior were observed between static and dynamic systems.

Corrosion kinetics

The corrosion behavior of the alloys was analyzed by fitting the weight gain with the equation.

$$W = At^n \qquad (1)$$

where W is the weight gain in mg/dm^2, t is the exposure time (days), while A and n are constants. One example of such a fit is shown in Figure 8. The corrosion examination test schedule was designed to gather a large number of data points in the early part of the corrosion process to ensure that the corrosion kinetics are well characterized. Table 2 summarizes the corrosion characteristics of the alloys in supercritical water and steam at 500°C. The values of n calculated from the fitting are reasonably consistent between the supercritical water static and dynamic autoclaves and only a little lower in

steam. This suggests that similar corrosion mechanisms are at work in the different environments.

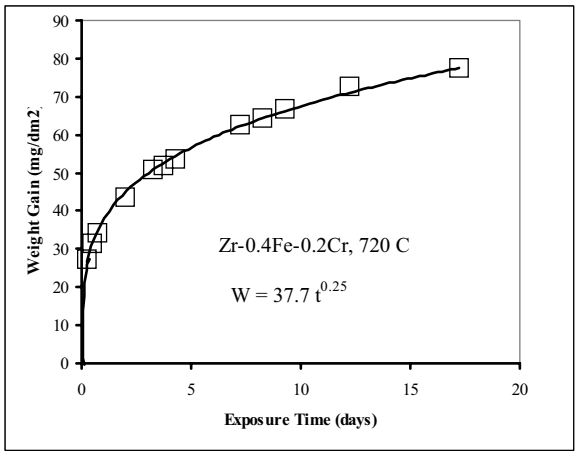

Figure 8: Power law fitting of corrosion weight gain versus exposure time for Zr-0.4Fe-0.2Cr alloy processed at 720°C .

The values of n indicate significantly lower than parabolic kinetics (n=0.5) as was also observed during corrosion of the same model alloys in 360°C water. The classical interpretation of such a result is that while solid state diffusion in the oxide layer is still the rate-limiting step for corrosion, other factors, such as lateral cracks or changing oxide grain size reduce the rate of diffusion in the oxide layer and decrease the value of n. It is not clear at this point what microstructure feature of the oxide causes this behavior. During corrosion testing in 360°C water, it was observed that the value of n was characteristic of the alloy. Comparing the actual values of n obtained in 360°C water with those obtained at 500°C , the hierarchy is similar (Zr-Nb alloys have the highest values of n, and ZrCrFe among the lowest) but the absolute values are a little higher in 500°C testing. Also of importance is the tendency of the oxides to lose their protectiveness (exhibit breakaway corrosion). It was found that this tendency was much more marked at 500°C , where more than half the alloys examined exhibited such behavior.

Corrosion Rates of Zr alloys compared to other alloys considered for the SCWR.

One of the design constraints is that the alloys to be used in the SCWR be resistant to uniform corrosion at high temperature. There are various alloys currently under consideration for the cladding material and structural components, including inconels, ferritic-martensitic alloys and stainless steels. In this section we compare the corrosion rates in Zr alloys at 500°C with other alloys. To compare within the same test conditions, a ferritic martensitic steel was tested in SCW in one of the autoclaves used for this test (static autoclave at KAERI). After 24 days, the corrosion weight gain was compared to the best alloys from each of the alloy groups considered in this study, and this is shown in Figure 9. From the figure it is clear that the overall weight gain of the F/M steel is higher than the best Zr based alloys. In addition, a detailed examination of the weight gain as a function of time showed early weight loss in the steel, indicating spalled oxide or oxide dissolution. This is shown in Figure 10. This means that for this particular case the weight gain for the F/M steel should be even higher than what is shown in Figure 9, since the oxide is not adherent. Therefore care needs to be taken in drawing comparisons between alloy corrosion weight gain at a single fixed point as these comparisons implicitly require that all oxide be adherent and that the oxidized metal be retained in the oxide.

A more detailed comparison can be performed with the results of other research programs of corrosion testing of candidate materials for the SCWR [11]. The data on corrosion weight gain of other alloys in 500°C SCW available to us is plotted in Figure 11, and compared to some of the better alloys in this study.

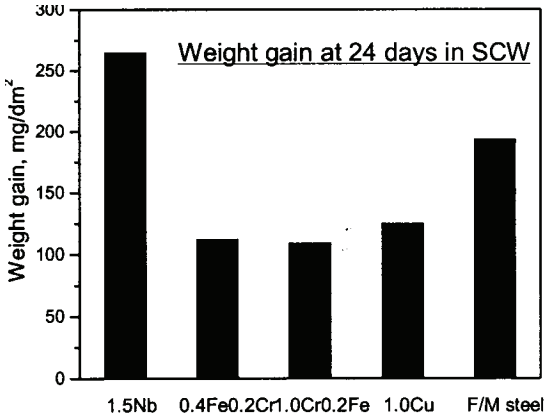

Figure 9: Weight gain after 24 days in supercritical water conditions for good-performing Zr alloys compared to a F-M steel exposed in the same autoclave.

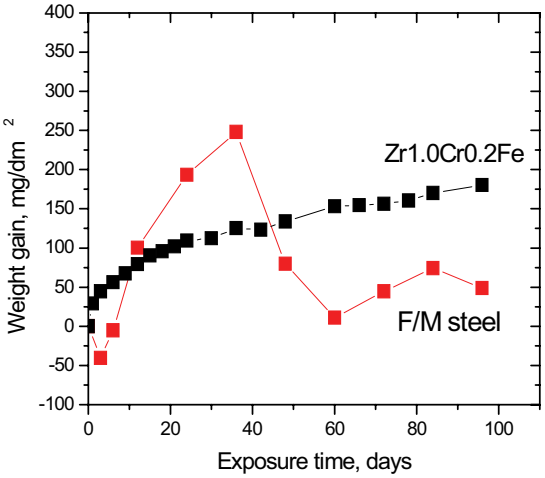

Figure 10: Weight gain versus exposure time comparison between ZrCrFe alloy and F/M steel in 500°C SCW.

Overall, the data available for Zr alloys is more extensive and spans a longer period of time than for the other alloys. The stainless steels show the lowest rates of uniform corrosion, although they are susceptible to stress corrosion cracking [12].

Table 2. Calculated pre-transition corrosion kinetic parameters A and n for the model alloys in SCW

Alloy	Condition	A	n
Zr0.4Cr0.2Fe (L)	SCW dynamic	25	0.38
	500 C steam	31	0.29
	SCW static		
Zr-0.4Fe-0.2Cr (H)	SCW dynamic	30	0.37
	500 C steam	37	0.28
	SCW static	35	0.36
Zr-0.5Cr-0.2Fe	SCW dynamic	32	0.32
	500 C steam	40	0.27
	SCW static		
Zr-1.0Cr-0.2Fe	SCW dynamic	38	0.30
	500 C steam	30	0.34
	SCW static	30	0.40
Zr-1.5Nb	SCW static	32	0.66
Zr-1.0Cu	SCW static	33	0.41

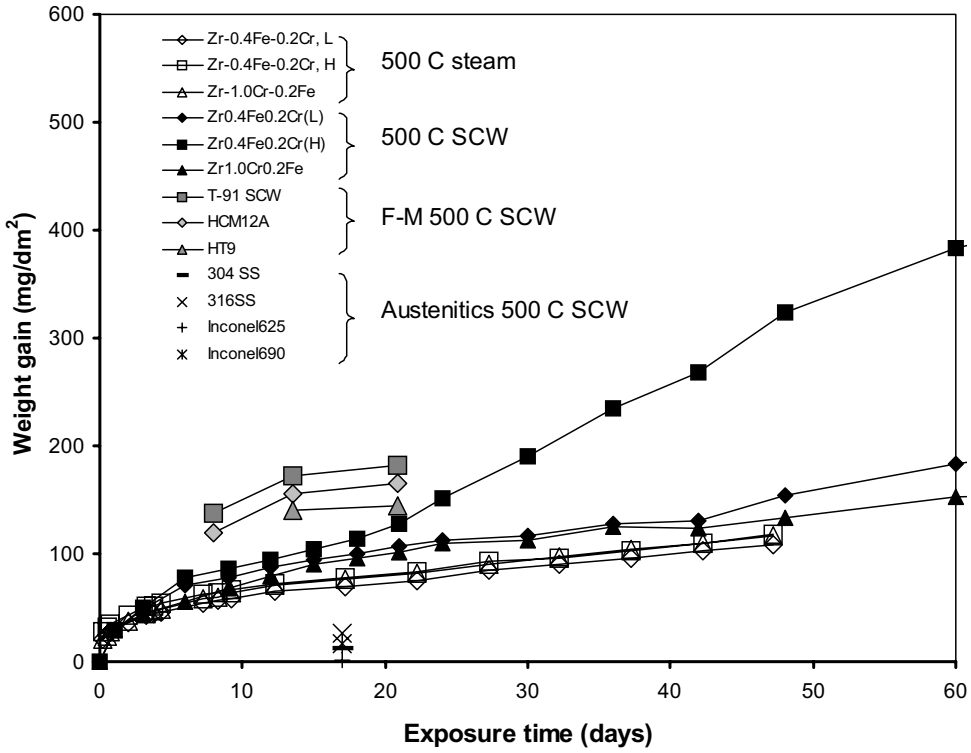

Figure 11: Weight gain versus exposure time in steam (open symbols) and supercritical water conditions (filled symbols), for good-performing Zr alloys and some of the other alloys currently under consideration for the SCWR.

For the testing times available for comparison, the Zr-based alloys show corrosion behavior that is comparable (and somewhat lower) than the ferritic-martensitic alloys. We note that weight gain is not a perfect indicator of corrosion behavior because of different stoichiometries of oxides formed on zirconium alloys and iron based alloys. However, because for an equivalent weight gain, more metal is consumed in the iron oxides than in zirconium oxides, the correction would improve the ranking of the zirconium alloys relative to iron oxides. These results suggest that, at least from a uniform corrosion point of view, Zr-based alloys deserve consideration for potential use in cladding and structural components for SCWR.

Conclusions

Corrosion tests in supercritical water and 500°C steam were performed on Zr-based model alloys up to 132 days to evaluate the potential use of Zr alloy cladding in the SCWR.

1. The corrosion test results showed a wide variety of corrosion resistance depending on the alloy composition. In general the best alloys were from the ZrCrFe system (which also behaved the best in 360 C water corrosion test). Higher alloying content improved corrosion resistance.

2. Results were consistent between static and dynamic autoclaves and showed a slightly higher rate in SCW as compared to 500°C steam. This suggests that static autoclave tests can be used to assess corrosion behavior at high temperature and that 500°C steam tests can be used as an effective screening test.

3. In comparison with other alloys being considered for the SCWR, the Zr alloys showed higher corrosion rates than austenitic alloys, and somewhat lower corrosion rates than ferritic-martensitic alloys, at least up to the times that these other alloys have been tested.

Ongoing research will characterize these oxide layers to rationalize the observed differences in corrosion behavior.

The results of this study imply that, at least from a corrosion standpoint, Zr alloys deserve consideration as potential cladding or structural materials in supercritical water cooled reactors.

Acknowledgments

This work was supported by a DOE I-NERI grant no. DE-FG07-03RL14530 and by MOST at KAERI. Use of the Advanced Photon Source was supported by the U.S. Department of Energy, Basic Energy Sciences, Office of Science, under Contract No. W-31-109-Eng-38. M. Gomes da Silva was a recipient of a scholarship from CNPq-Brazil for his doctoral study, for the duration of this project.

References

[1] D. L. Douglass, *The Metallurgy of Zirconium*. Vienna: International Atomic Energy Agency Supplement, 1971.

[2] E. Gulbransen and K. F. Andrew, "Oxidation of Zirconium Alloys in Water Vapor Atmospheres Containing Trace Amounts of Oxygen at 375 ° and 575°C," *Electrochemical Technology*, vol. 4, pp. 99, 1966.

[3] J. Bolton, "The Corrosion of Zirconium Alloys," in *Corrosion of Reactor Materials II*. Vienna: IAEA, 1962, pp. 133.

[4] H. H. Klepfer, "Zirconium Alloy Design for Steam Service," GEAP-4089 Vol.1, 1962.

[5] K. T. Erwin, O. Delaire, A. T. Motta, R. C. Birtcher, Y. Chu, and D. Mancini, "Observation of second-phase particles in bulk zirconium alloys using synchrotron radiation," *Journal of Nuclear Materials*, vol. 294, pp. 299-304, 2001.

[6] D. Shaltiel, I. Jacob, and D. Davidov, *Journal of the less-common metals*, vol. 53, pp. 117-131, 1976.

[7] D. Charquet, R. Hahn, E. Ortlieb, J.-P. Gros, and J.-F. Wadier, "Solubility Limits and Formation of Intermetallic Precilitates in ZrSnFeCr Alloys," Zirconium in the Nuclear Industry: 8th International Symposium, 1989, ASTM, STP 1023, 405-422.

[8] Y. H. Jeong, H. G. Kim, and T. H. Kim, *Journal of Nuclear Materials*, vol. 317, pp. 1, 2003.

[9] H. G. Kim, Y. H. Jeong, and T. H. Kim, *Journal of Nuclear Materials*, vol. 326, pp. 125, 2004.

[10] P. Barberis, E. Ahlberg, N. Simic, D. Charquet, M. Dahlback, M. Limback, P. Tagstrom, C. Lemaignan, G. Wikmark, and B. Lehtinen, "The role of second phase particles in binary zirconium alloys," 13th International Symposium on Zirconium in the Nuclear Industry, Annecy, France, 2002, ASTM, STP 1423, 33.

[11] G. S. Was, S. Teysseyre, and J. McKinely, "Corrosion and Stress Corrosion cracking of Iron and Ni base austenitic alloys in Supercritical Water," Corrosion 2004, New Orleans, 2004, NACE International, paper # 4492.

[12] G. S. Was and T. R. Allen, "Time, Temperature, and Dissolved Oxygen Dependence of Oxidation in Austenitic and Ferritic-Martensitic Alloys in Supercritical Water," International Congress on Advances in Nuclear Power Plants, Seoul, Korea, 2005.